Computational Study of the Reaction SH + O_2

Chenlai (Ryan) Zhou, Karina Sendt,* and Brian S. Haynes

School of Chemical and Biomolecular Engineering, University of Sydney, NSW 2006, Australia

Received: November 17, 2008; Revised Manuscript Received: December 29, 2008

The reaction of SH + O_2 has been characterized using multireference methods, with geometries and vibrational frequencies determined at the CASSCF/cc-pVTZ level and single-point energies calculated at the MRCI/aug-cc-pV(Q+*d*)Z level. The dominant product channels are found to be SO + OH and HSO + O. Whereas the formation of SO + OH has a barrier of ~81 kJ mol^{-1}, it is energetically more favorable than the formation of HSO + O, which is barrierless beyond the endothermicity of ~89 kJ mol^{-1} at 0 K. Thus, the reaction SH + O_2 → SO + OH is 2 orders of magnitude faster than the reaction SH + O_2 → HSO + O at room temperature, revealing that the atmospheric oxidation of SH leads directly to the formation of SO + OH with the rate coefficient of ~1.0×10^{-2} cm^3 mol^{-1} s^{-1}. At temperatures above 1000 K, however, the rates of the two channels become comparable. This may be attributed to the entropy effects leading to the higher pre-exponential factor for the channel (forming HSO + O) via a more loose transition state than that (forming SO + OH) entailing a four-centered transition state. Whereas the hydrogen abstraction reaction producing S + HO_2 is found to proceed on the quartet surface, the substantial barrier of ~165 kJ mol^{-1} means that it occurs as a minor product channel. Finally, the formation of possible products SO_2 + H is prohibited due to the lack of a transition state for the direct sulfur insertion.

1. Introduction

The kinetics of the reaction SH + O_2 are important in describing the behavior of sulfur in both the atmospheric oxidation sequence and in the combustion of H_2S, such as occurs in the Claus process. The possible bimolecular product channels are:

$$SH + O_2 \rightarrow \text{products} \quad \text{(R1)}$$

$$\rightarrow SO_2 + H \qquad \Delta H_{0K} = -220 \text{ kJ mol}^{-1} \quad \text{(R1a)}$$

$$\rightarrow SO + OH \qquad \Delta H_{0K} = -100 \text{ kJ mol}^{-1} \quad \text{(R1b)}$$

$$\rightarrow HSO + O \qquad \Delta H_{0K} = 87 \text{ kJ mol}^{-1} \quad \text{(R1c)}$$

$$\rightarrow S + HO_2 \qquad \Delta H_{0K} = 148 \text{ kJ mol}^{-1} \quad \text{(R1d)}$$

With respect to direct measurements of the rate coefficient of R1, only upper limits at room temperature have been reported to date.[1−5] In early mechanism development,[6] two exothermic product channels (R1a and R1b) were first introduced with crude estimates of their rate coefficients. In their kinetic analysis of the H_2S reaction in flash-photolysis shock tube experiments, Tsuchiya and co-workers[7] suggested that the additional product channels R1c and R1d were more likely than R1a and R1b to occur as elementary reactions. The large endothermicity of R1d meant that it could safely be ignored in the analysis of their data, obtained in the temperature range of 1400−1850 K, but they included the other three channels in their mechanism development.[7] Through fitting model predictions for the concentrations of O and H atoms with experimental results, they concluded that R1c was the only important channel of reaction 1. Tsuchiya et al.[7] also reported theoretical work that indicated that the formation of HSO + O has no barrier beyond its endothermicity and is kinetically favorable.

In contemporaneous theoretical calculations on the H/S/O/O system,[8,9] Goumri and co-workers identified an intermediate adduct HSOO with energy 26 kJ mol^{-1} lower than the SH + O_2 asymptote and concluded that R1c occurred via this adduct through two unimolecular channels:

$$SH + O_2 \rightarrow HSOO \qquad \Delta H_{0K} = -26 \text{ kJ mol}^{-1} \quad \text{(R2)}$$

$$HSOO \rightarrow HSO + O \qquad \Delta H_{0K} = 112 \text{ kJ mol}^{-1} \quad \text{(R3)}$$

Whereas a substantial barrier was found for reaction R2 at the MP2/6-31G* level, further single-point calculations at the G2 level suggested that it was also barrierless and the barrier obtained at the MP2/6-31G* level was attributed to spin contamination. An RRKM approach in conjunction with variational transition state theory was therefore used to derive the rate coefficients for R2 and R3. The formation of HSOO was found to be equilibrated at room temperature or above, and the effective rate coefficient for R1c was therefore evaluated as the product of the rate coefficient for R3 at the high-pressure limit and the equilibrium constant for reaction R2. This analysis yielded a value for the rate of R1c one order of magnitude higher than that deduced by Tsuchiya et al.[7] The high value of the calculated rate coefficient arises from the variational treatment of a loose transition state, which leads to a large entropy change in the reaction R3 and hence to a high value for the pre-exponential factor (4.9×10^{14} cm^3 mol^{-1} s^{-1}). However, given the presence of multireference character arising from near-degenerate configurations for doublet and quartet states in the bond fission process (R3), the potential energy surface (PES) along the reaction coordinate may be poorly characterized at the G2 level, leading to significant uncertainty in the estimated rate coefficient.

In an effort to study the kinetics of reaction R2 using multiconfigurational methods, Resende and Ornellas[10] performed

* Corresponding author e-mail: k.sendt@usyd.edu.au.

10.1021/jp810105e CCC: $40.75
Published on Web 02/16/2009

CASSCF and CASPT2 calculations with an active space of 9 electrons distributed among 10 orbitals or fewer. A pronounced barrier (~52 kJ mol^{-1}) was found to separate the reactants and products for reaction R2. The structure of the transition state is similar to that determined at MP2 level[8] except for the relatively longer S−O bond length (2.3 Å vs 2.0 Å). Additionally, a four-centered transition state responsible for isomerization of HSOO to HOOS was located for the first time − decomposition of HOOS leads to the formation of SO + OH, suggesting that reaction R1b could be an important product channel. Whereas a substantial barrier close to the endothermicity of R1d (i.e., ~150 kJ mol^{-1}) was reported for R1b, this result may be unreliable because of the use of single-reference methods for characterization of this transition state with the geometry and single-point energy determined at MP2/cc-pVTZ and CCSD(T)/CBS levels, respectively.

More recently, a global PES for the H/S/O/O system was generated by the double many body expansion (DMBE) approach, using the global minimum and some local minima and saddle points characterized at the CASSCF level.[11] According to the 2D contour plots, a van der Waals minimum corresponding to HSO···O was found with energy similar to that of stable intermediate HSOO (i.e., ~80 kJ mol^{-1} lower than HSO + O). Whereas early theoretical studies suggested the absence of the transition state directly leading to the formation of SO_2 + H,[8,10] the existence of this van der Waals complex opens up the possibility for reaction R1a to proceed via isomerization to the intermediate HSO_2, followed by its dissociation to products SO_2 + H. A dynamic study was performed for reaction R1 on the DMBE surface, treating SH in both the ground-state and several vibrationally excited states.[12] Specific rate coefficients with respect to SH disappearance in different vibrational states were produced from trajectory simulations, indicating that HSO + O are the major products except for situations in which the total system energy is either below the threshold for producing HSO + O or above the bond cleavage limit of SH, in which cases the formation of SO_2 + H dominates.

Because there are large uncertainties in measurements[7] as well as contradictions in theoretical studies,[8,10,12] the present work aims to elucidate the chemistry of reaction R1 using high-level computational methods. Given the success in characterizing sulfur systems in recent work,[13,14] the multireference configuration interaction (MRCI) level of theory is employed to compensate for the shortcoming of the CASSCF method with respect to the dynamical correlation. All possible bimolecular product channels except H + SOO for the reaction R1 are considered, and three-parameter Arrhenius expressions are derived for those kinetically favored.

2. Computational Methods

2.1. Characterizing the Potential Energy Surface. The PES for reaction R1 was characterized on the doublet ground surface using multiconfigurational methods with full valence active space containing 19 electrons distributed in 13 orbitals (unless otherwise noted). To perform geometry optimizations at the MRCI level for a system with this active space requires substantial computational expense. As an alternative, the equilibrium geometries of stable molecules and transition states were optimized at the CASSCF/cc-pVTZ level of theory. Subsequent single-point energy calculations were performed at the MRCI/aug-cc-pV(Q+*d*)Z level of theory. For the MRCI energy, the Davidson correction[15] was applied to approximate the CI energy up to quadruple excitations (CISDTQ). The correlation-consistent basis set with the more balanced *d*-function set modified by Dunning et al.[16] was used as it allows better characterization of systems containing second-row atoms such as sulfur.[17] To overcome the lack of size consistency in the MRCI calculation, the energy asymptote for bimolecular reactants and products were calculated as a superadduct with the stable molecules being separated by a distance of 50 Å. Trial calculations shows that the nonconsistency of MRCI introduces an error of ~25 kJ mol^{-1} for SH + O_2. Harmonic vibrational frequencies and the zero-point vibrational energy (ZPVE) of stable molecules and transition states were calculated analytically at the CASSCF/cc-pVTZ level. Previous work on the H/S/O system shows that these values can be reasonably predicted without the use of any additional scaling factor.[13]

The electronic and relative energies (including ZPVE correction) for stable molecules and transition states are presented in Table 1. Detailed geometry parameters and vibrational frequencies are contained in the Supporting Information. The quantum chemistry calculations were performed using *Molpro*,[18] *Dalton*,[19] and *Gaussian 98*[20] packages.

2.2. Kinetics. The rate coefficients for significant product channels in reaction R1 were evaluated by transition state theory (TST) with vibrational partition functions computed using the harmonic oscillator assumption. For reactions with a substantial barrier, the tunnelling effect was estimated according to Wigner's formulation.[21] Alternatively, when a reaction showed no significant barrier, the transition states were selected variationally along the reaction coordinate to identify the minimum rate coefficient. The Arrhenius expression in three-parameter form was then derived by the use of a least-squares fit over the temperature range from 300 to 2000 K.

3. Results and Discussion

3.1. Potential Energy Surface. The PES for the reaction R1 is depicted in Figure 1, which includes bimolecular product channels R1b, R1c, and R1d. Part (a) of Figure 1 shows the three channels at the CASSCF level (at which the geometries were optimized), whereas part (b) of Figure 1 shows the MRCI energies at the CASSCF stationary points. Except for the products HSO + O and S + HO_2, the relative energies of the stable species and the relative heights of the barriers beyond the endothermicity differ significantly between the two methods. It is clear that the MRCI energies relative to SH + O_2 are lower than the corresponding energies predicted by the CASSCF method. The lack of the dynamical correlation at the CASSCF level is responsible for its quantitative inaccuracy even for stable species at their equilibrium geometries, highlighting the need for this method to produce a reliable PES and hence reaction kinetics. The geometry parameters of tetratomic intermediates and transition states involved are shown in Figure 2. As an indication of the reliability of the computational methods employed, Table 1 includes relative energies calculated from G3 energies and from reported heats of formation for stable species. The overall discrepancy is found to be within ~12 kJ mol^{-1}, with the exception of HSOO for which significantly lower values are predicted at G2[22] and G3 levels. However, the T1 diagnostic factor of 0.0336 reported in the G3 calculation and the largest CI coefficient of 0.964 gained at the CASSCF level indicate that the single-reference treatment may not be adequate for accurate characterization of this species. This may be attributed to the relatively longer S−O bond of ~1.7 Å than a typical length of ~1.5 Å such as the one in the analogous species HSO.[13] The low S−O bond dissociation energy (1.3 kJ mol^{-1}) determined at the MRCI level implies that the formation

TABLE 1: Electronic and Relative Energies (inc. ZPVE correction) of the Optimized Reactants, Products, Intermediates, and Transition States in the Reaction SH + O_2

	electronic energies (a.u.)		ZPVE (a.u.)	relative energies (0 K) to SH + O_2 (kJ mol^{-1})			
species	CASSCF[a]	MRCI[b]	CASSCF[a]	CASSCF[c]	MRCI[c]	G3	lit. values
SH	−398.11831754		0.005888				
O_2	−149.75742420		0.003502				
SH + O_2	−547.87574174	−548.47170845	0.009390	0	0	0	0[d]
HSO	−473.04007371		0.010696				
O	−74.80564442		0.000000				
HSO + O	−547.84571813	−548.43935778	0.010696	82.3	88.4	81.3	86.9 ± 1.1[d]
SO	−472.45076759		0.002413				
OH	−75.43930589		0.008317				
SO + OH	−547.89007348	−548.50660366	0.010730	−34.1	−88.1	−103.3	−99.6± 2.1[d]
HO_2	−150.32000173		0.013854				
S	−397.50361236		0.000000				
HO_2 + S	−547.82361409	−548.41823404	0.013854	148.6	152.1	145.8	148.0 ± 1.3[d]
HSOO	−547.87380189	−548.47668715	0.013867	16.8	−1.3	−17.0	−26.1[e]
cis-HOOS	−547.88027681	−548.50187698	0.015896	5.2	−62.1		
trans-HOOS	−547.88218412	−548.50335254	0.015697	−0.4	−66.5	−71.3	−78.5[e]
TS1	−547.86152329	−548.47563935	0.011322	42.4	−5.2		
TS2	−547.84114641	−548.44047023	0.011991	97.7	88.8		
TS3	−547.82189198	−548.44257682	0.011192	146.1	81.2		
TS4	−547.87999271	−548.50127505	0.015484	4.8	−61.6		
TS5	−547.88013397	−548.50341947	0.013767	0.0	−71.8		
^{2}TS6	−547.79258056	−548.40051588	0.008102	215.0	183.5		
^{4}TS6	−547.80011992	−548.40764296	0.008261	195.6	165.2		

[a] Geometry optimizations and frequency calculations performed at the full valence CASSCF/cc-pVTZ level. [b] Single-point energy calculations at the full valence active space MRCI+Davidson/aug-cc-pV(Q+*d*)Z level. [c] Electronic energies and ZPVE taken from a and b. [d] 0 K values extrapolated from literature $\Delta H_f°_{298}$ for SH,[26] O_2,[25] HSO,[27] O,[25] SO,[25] OH,[27] HO_2[27] and S.[25] [e] 0 K values extrapolated from G2 $\Delta H_f°_{298}$.[22]

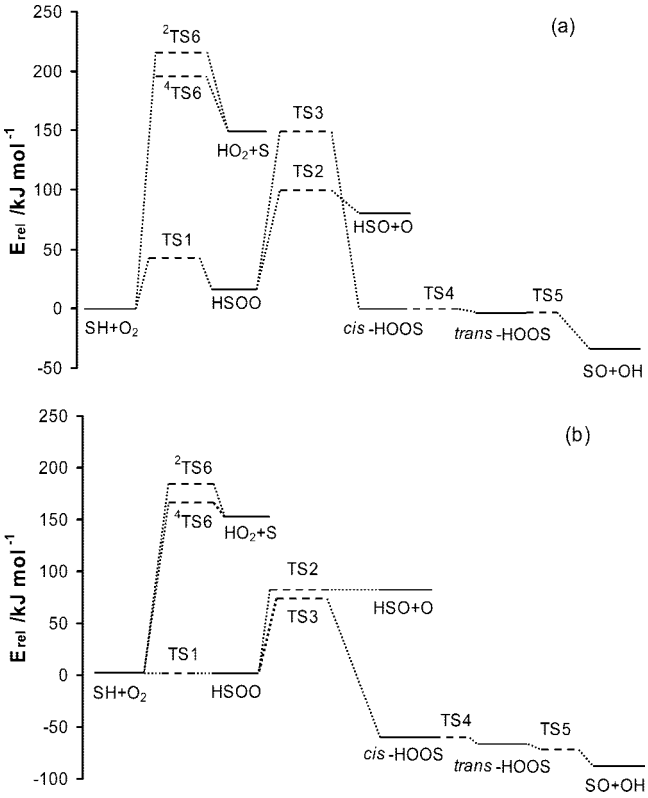

Figure 1. Potential energy diagram for the reaction SH + O_2: (a) Characterized at the full valence CASSCF/cc-pVTZ level of theory, including ZPVE correction; (b) single-point energy calculations performed at the full valence active space MRCI+Davidson/aug-cc-pV(Q+*d*)Z level of theory using CASSCF geometries and ZPVE correction.

of HSOO is thermodynamically even less favorable than early predictions had indicated.[9]

For the reaction R2, a transition state (TS1) with a substantial barrier (~42 kJ mol^{-1}) was found at the CASSCF level, in good agreement with previous studies.[8,10,11] However, at the MRCI level, the electronic energy of TS1 is reduced and actually lies 10.2 kJ mol^{-1} below the asymptote for SH + O_2, which is similar to the situation found with G2 calculations.[8] This may imply that TS1 may not be located at a saddle point and that it would need to be located variationally if accurate kinetic parameters were required. Whereas TS1 is somewhat higher than HSOO in MRCI energy on the electronic surface, the ZPVE contribution flattens the PES in the vicinity of SH + O_2, TS1, and HSOO, at least within the error of the current method. Overall, the present work supports the conclusion that reaction R2 is barrierless.

The product channel R1c includes the dissociation of HSOO to HSO + O (i.e., R3). However, in contrast to earlier work,[8,10,11] a transition state (TS2) was identified for the reaction R3, with a much shorter O−O bond length than found previously (~1.9 Å vs ~2.7 Å).[8] Whereas there is a substantial reverse barrier for R3 at the CASSCF level, this reduces to only 0.4 kJ mol^{-1} at the MRCI level, suggesting that any barrier for R3 beyond the endothermicity is likely to be small.

In an effort to locate TS2 variationally, it is necessary to obtain a reliable PES along the reaction coordinate of R3. This was achieved by performing partial optimizations at the CASSCF/cc-pVTZ level for a series of frozen O−O separations increasing from that of equilibrium HSOO (~1.35 Å) to 4 Å. The corresponding vibrational frequencies were calculated at the same level of theory. To ensure the reliability of these optimized geometries, additional partial optimizations were performed at the MRCI/cc-pVTZ level of theory for the points of interest. However, because of the lack of analytical gradient for geometry optimizations at the MRCI level, the gradient is instead calculated numerically, but this is computationally prohibitive when performing the full valence optimization in

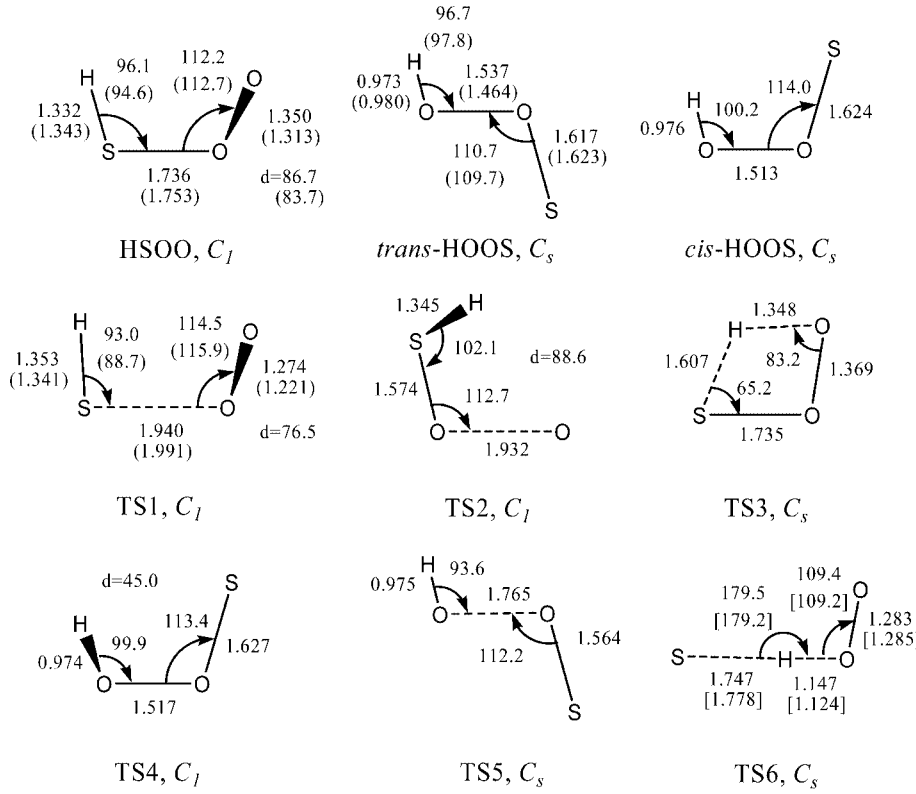

Figure 2. Equilibrium geometry parameters optimized at the full valence CASSCF/cc-pVTZ level of theory for intermediates and transition states involved in the reaction SH + O_2. Values shown in parentheses () are optimized at the MP2(full)/6-31G* level.[8,22] Values shown in brackets [ ] are optimized on the quartet surface in the present work. Bond lengths and angles are given in Å and degrees, respectively.

TABLE 2: Partially Optimized Geometries in the Reaction Coordinate of HSOO → HSO + O[a]

		r(S−O)		r(S−H)		a(H−S−O)		a(O−O−S)		d(O−O−S−H)	
species	r(O−O)	CASSCF	MRCI	CASSCF	MRCI	CASSCF	MRCI	CASSCF	MRCI	CASSCF	MRCI
HSOO	1.350	1.736		1.332		96.1		112.2		86.7	
	1.4	1.720		1.332		96.6		111.3		87.0	
	1.6	1.674		1.334		98.2		109.3		87.5	
	1.7	1.647		1.336		99.2		109.4		87.7	
	1.8	1.614	1.582	1.339	1.344	100.4	100.7	110.5	111.2	88.1	88.2
TS2	1.932	1.574	1.547	1.345	1.350	102.1	102.4	112.7	112.9	88.6	88.6
	2.0	1.560	1.537	1.347	1.352	102.8	102.9	113.9	113.6	88.8	88.8
	2.1	1.547	1.528	1.350	1.354	103.4	103.5	115.4	114.6	88.9	88.8
	2.2	1.539	1.523	1.352	1.355	103.8	103.8	116.7	115.4	88.9	88.7
	2.3	1.535	1.520	1.353	1.356	104.1	104.0	117.8	116.1	88.6	88.4
	2.4	1.532		1.353		104.3		118.7		88.4	
	2.7	1.529		1.354		104.5		120.3		85.6	
	3.0	1.529		1.354		104.4		101.6		0.0	
HSO···O	3.223	1.529		1.354		104.4		97.9		0.0	
	3.5	1.529		1.354		104.5		93.4		0.0	
	4.0	1.529		1.354		104.5		84.0		0.0	
HSO + O	∞	1.528		1.355		104.6		-		-	

[a] CASSCF and MRCI represent optimizations performed at the full valence CASSCF/cc-pVTZ level and the reduced active space (9 electrons, 8 orbitals) MRCI/cc-pVTZ level, respectively. Bond lengths and angles are given in angstroms and degrees, respectively.

this work. To reduce the computational expense significantly while still maintaining the reliability of MRCI optimization, five doubly occupied valence orbitals, each with occupation number greater than 1.997 in the full valence CASSCF calculations, were selected to be downgraded into inactive space, such that the size of the active space was reduced to 9 valence electrons distributed in 8 orbitals. Using initial geometries optimized at the CASSCF level, the electronic energies were reduced by ∼1 kJ mol^{-1} after the optimization at the MRCI level. The discrepancy is less than 2% with respect to the geometry variation, as shown in Table 2, indicating that the CASSCF level accurately reproduces the MRCI transition state geometries for reaction R3. Thus, for the points of interest, subsequent single-point energy calculations were performed at the MRCI+Davidson/aug-cc-pV(Q+*d*)Z level of theory using CASSCF geometries.

Figure 3 shows the slice of the PES for the reaction R3 at the full valence MRCI level (using CASSCF geometries) and the reduced active space MRCI level along with CASSCF energies scaled to give the heat of reaction at the full valence MRCI+Davidson/aug-cc-pV(Q+d)Z level for comparison. Whereas the CASSCF PES shows an apparent barrier, the MRCI PES characterized using both the reduced active space and the full valence active space indicates that it is negligibly small. The agreement between the full valence and reduced active

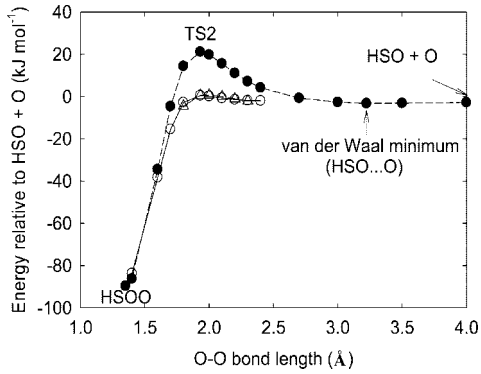

Figure 3. Slice of the PES for the reaction coordinate of HSOO → HSO + O showing equilibrium points for HSOO, TS2, and HSO···O and transition states connecting these. Solid circles show the scaled PES characterized at the full valence CASSCF/cc-pVTZ level. Open triangles and open circles show the PES characterized at the reduced active space MRCI/cc-pVTZ level and the full-valence active space MRCI+Davidson/aug-cc-pV(Q+*d*)Z level using CASSCF geometries, respectively. ZPVE corrections were determined at the CASSCF/cc-pVTZ level.

space absolute energies are within 1 kJ mol^{-1}, indicating that the reduced active space is a good approximation of the full valence energies in the vicinity of TS2. In addition to the equilibrium geometries for HSOO and TS2, a van der Waals minimum (HSO···O) was obtained when relaxing the restriction on the O−O separation. The O−O bond length is significantly longer than that arising on the DMBE surface[11] (3.2 Å vs 2.1 Å). Not surprisingly, we also find the energy of HSO···O to be closer to (∼3 kJ mol^{-1} below) the asymptote of HSO + O than is shown on the DMBE surface[11] (where the energy is actually closer to that of HSOO).

An attempt was made to extend the MRCI energy to the larger O−O separation in Figure 3. However, due to convergence difficulties at extended bond lengths where the fragments were interacting (i.e., van der Waals complexes), this was not possible.

An alternative fate of HSOO is the isomerization to the more stable intermediate HOOS followed by dissociation to SO + OH, completing product channel R1b. A four-centered transition state (TS3) was found to connect HSOO and *cis*-HOOS. Whereas its geometry is staggered with the dihedral angle of 23° at the MP2 level,[10] it becomes planar at the CASSCF level. Prior to dissociation to SO + OH, *cis*-HOOS undergoes rotational isomerization to the more stable *trans*-HOOS, overcoming a negligible barrier (TS4) of 0.5 kJ mol^{-1} in the process. Because TS5 lies at an electronic energy intermediate between *trans*-HOOS and SO + OH at the MRCI level, it is probable that *trans*-HOOS is not stable, in accordance with results from G2[8] and reduced active-space CASPT2 calculations.[10] Thus, the overall barrier for R1b is determined by TS3. In contrast to early estimates of the barrier height,[7,8] we find the MRCI energy of TS3 to be slightly lower than that of TS2 by ∼8 kJ mol^{-1}, although within the uncertainty of the current method (∼12 kJ mol^{-1}). It should be noted that the MRCI energy using the reported staggered MP2 geometry[10] is ∼59 kJ mol^{-1} higher than that using the CASSCF geometry. Furthermore, the largest CI coefficient of 0.943 gained at the CASSCF level suggests that the single-reference method (MP2) is not adequate to predict the geometry of TS3 and hence it is the CASSCF geometry that we adopt here. Nevertheless, the relatively low barrier height obtained for TS3 in this work suggests that channel R1b may compete with R1c at low temperatures in particular.

Despite the high endothermicity of reaction R1d (∼152 kJ mol^{-1}), we have for completeness characterized the direct H abstraction on both the doublet and quarter surfaces. Transition states are located at MRCI barrier heights 183 (doublet) and 165 kJ mol^{-1} (quartet), confirming that reaction R1d is too slow to be an important product channel for R1. We have not considered the formation of SOO + H, which has much higher endothermicity than R1d.[9]

Lastly, we attempted to locate a transition state leading to the formation of HSO_2 or its effective bimolecular products SO_2 + H (R1a). However, the first order saddle point optimization eventually converged to TS2 instead. This agrees with an early theoretical study,[8] suggesting that a direct transition state may not exist for R1a. Here, we note that Ballester and co-workers[11] recently reported a transition state (with energy well below that of HSO + O) separating the van der Waals minimum HSO···O and HSO_2. According to their PES, HSO···O is more than 80 kJ mol^{-1} lower than HSO + O, which is most unexpected for a van der Waals complex. In an effort to validate the reliability of their DMBE surface, we performed geometry optimizations on the reported geometries for HSO···O and their transition state at the same level of theory (CASSCF/aug-cc-pVDZ) as they had employed for stationary points. We found that both geometries were not even close to stationary points with gradients greater than 0.057 and 0.068 and electronic energies ∼29 kJ mol^{-1} and ∼39 kJ mol^{-1} respectively above the asymptote of HSO + O. As the optimization continues, the O−O bond in both geometries falls apart, leading to the formation of HSO + O. This result suggests that the PES generated by the DMBE interpolation procedure has not reliably described the PES, at least in the vicinity of the channel apparently leading to HSO_2.

3.2. Kinetics. According to the PES shown in Figure 1, the significant product channels for the reaction R1 are the decompositions of the adduct HSOO leading to the formation of SO + OH (R1b) and HSO + O (R1c). Here, we derive apparent kinetic rate coefficients for the overall processes using MRCI energies without scaling. The very low barriers for the forward and reverse of reaction R2 mean that this reaction is equilibrated under any conditions of practical interest. Therefore, the partition functions for HSOO as a reactant have been taken directly as those for SH and O_2.

The rate-limiting step in the formation of SO + OH is to surmount the barrier of TS3, after which weak chemical bonding allows multiple rearrangements without significant stabilization. We therefore apply TST to TS3, obtaining the three-parameter Arrhenius expression for the overall product channel R1b:

$$k_{\mathrm{R1b}} = 7.5\times10^{4}T^{2.052}\exp(-68.6\mathrm{kJ\ mol^{-1}}/RT)\ \mathrm{cm^{3}mol^{-1}s^{-1}}$$

The tunnelling effect accounts for a factor of between 5 and 2 at 300−600 K, decreasing to ∼1.4 at 1000 K and ∼1.1 at 2000 K.

The present MRCI PES is expected to provide a more reliable basis for the derivation of the rate coefficient of reaction R3 than the earlier theoretical study[8] with geometries and frequencies estimated according to the Gorin model[23] and energies characterized using a single-reference method (G2). According to Figure 3, the energy as a function of bond length reaches a maximum at the O−O separation of ∼1.9 Å. Thus, the rate coefficient was derived variationally using the transition states around that separation (1.7−2.1 Å). The harmonic assumption made in TST is still valid, given the occurrence of severe steric hindrance for the torsional mode corresponding to the lowest vibrational frequency of 217 cm^{-1} in the transition state.

As shown in Table 3, the minimum rate coefficients are found at TS2 in the temperature range 300−1600 K, whereas at higher

TABLE 3: Rate Coefficients (cm^3 mol^{-1} s^{-1}) for Different Transition State Geometries in the Reaction Coordinate of SH + O_2 → HSO + O

r(O−O)	temperature (K)				
(Å)	300	500	1000	1600	2000
1.7	9.03×10^{-2}	1.16×10^{4}	1.34×10^{8}	6.75×10^{9}	2.84×10^{10}
1.8	5.98×10^{-4}	5.92×10^{2}	3.18×10^{7}	2.84×10^{9}	1.45×10^{10}
1.932	1.90×10^{-4}	3.30×10^{2}	2.71×10^{7}	2.84×10^{9}	1.53×10^{10}
2.0	2.41×10^{-4}	4.09×10^{2}	3.29×10^{7}	3.42×10^{9}	1.84×10^{10}
2.1	4.02×10^{-4}	6.14×10^{2}	4.57×10^{7}	4.62×10^{9}	2.46×10^{10}

temperatures they are found at a more compact transition state. This analysis yields the Arrhenius expression for the product channel R1c

$$k_{R1c} = 2.3 \times 10^{6} T^{1.816} \exp(-83.7\text{kJ mol}^{-1}/RT)\ \text{cm}^3\text{mol}^{-1}\text{s}^{-1}$$

Figure 4 is an Arrhenius plot of rate constants for SH + O_2 channels derived here and reported in the literature. Our results show that R1b (forming SO + OH) is the dominant channel at temperatures below 1000 K; above that temperature, R1c (forming HSO + O) becomes competitive due to the higher pre-exponential factor for this reaction.

Our prediction of the rate of HSO + O formation via the reaction R1c is more than 2 orders of magnitudes slower than that derived in an early theoretical study.[8] This large discrepancy can be attributed to the relatively compact structure of TS2 in the present work (O−O separation ∼1.9 Å vs ∼2.7 Å), leading to a smaller reaction entropy change and hence to a lower pre-exponential factor.

Another theoretical rate coefficient chosen for comparison in Figure 4 is derived from the recent dynamic simulations of vibrational-state-specific SH consumption by reaction with ground-state O_2 molecules.[12] To facilitate comparison, the thermal rate coefficient was estimated assuming a Boltzmann distribution of vibrational states and the reported state-specific rate coefficients[12] up to the vibrational level 5 with values for the vibrational level 2 and 4 being interpolated. Here, it should be noted that, with the vibrational frequency for SH taken to be 2712 cm^{-1},[24] the population is dominated by the ground vibrational state, which accounts for more than 98% of the population at temperatures below 1000 K and ∼86% at 2000 K. However, we could not calculate a true thermal rate constant because the dynamic study included O_2 only in the ground state[12] − the relatively low vibrational frequency for O_2 (1580 cm^{-1})[25] leads to ground-state populations of ∼90% at 1000 K and ∼68% at 2000 K. Nevertheless, we have included the results of our calculations in Figure 4 as curve 3.

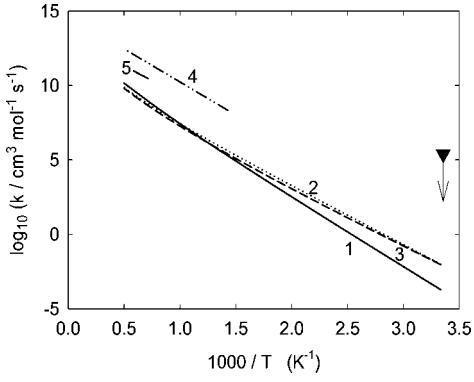

Figure 4. Rate coefficient comparison for product channels in the reaction SH + O_2: (1) SH + O_2 → HSO + O, present work; (2) SH + O_2 → SO + OH, present work; (3) SH + O_2 → products, using the approximate thermal distribution (text); (4) SH + O_2 → HSO + O, Goumri et al.;[8] (5) SH + O_2 → HSO + O, Tsuchiya et al.;[7] (▼) experimental upper limit at 298 K for SH + O_2 → products, Stachnik and Molina.[4]

The pseudothermal rate constant represented by curve 3 in Figure 4 is for the overall reaction R1 but should be compared with our results for channel R1c (curve 1) because HSO + O was the dominant product channel except at low and very high reactant energies in the dynamical study.[12] There is clearly very good agreement between curves 1 and 3 at high temperatures (700−2000 K), but at lower temperatures the activation energy implied by curve 3 falls well below the reaction endothemicity− we assume this to be a manifestation of the low-energy channel found in the dynamical calculations to lead to H + SO_2. However, as discussed above, we believe the appearance of this channel to be an artifact of the method used to generate the PES for the dynamical calculations. It is important to note here that the apparent coincidence of curves 2 and 3 in the low-temperature region is purely coincidental, as the product channel R1b was not accessed in the trajectory calculations. The failure to report this channel is the result of a further problem with the surface used in ref 12, namely the absence of both the intermediate species HOOS and TS3. In fact, calculations show that HOOS and TS3 can be identified using their methods (CASSCF/aug-cc-pVTZ for the stable species and CASSCF/aug-cc-pVDZ for the transition state). The geometries and relative energies are very close to those obtained at the similar level of theory (CASSCF/cc-pVTZ) in the present work. It is possible that HOOS and TS3 were not considered for the generation of the DMBE surface because the formation of SO + OH through this channel entails a higher barrier than reaction via the artifactual complex HSO···O, as discussed above.

There is only one experimental value with which we can meaningfully compare our results, namely the model-dependent expression of Tsuchiya et al.[7] obtained from shock-tube studies in the temperature range of 1400 −1850 K (curve 5 in Figure 4). Our value is 1 order of magnitude lower than that of Tsuchiya et al.,[7] an observation that we attribute to the early state of development of kinetic modeling of H_2S oxidation at the time that the experimental work was undertaken.

4. Conclusions

The reaction between SH and O_2, characterized at the MRCI level, occurs via the decomposition of the unstable intermediate adduct HSOO. The direct channel to produce S + HO_2 has a high barrier (∼165 kJ mol^{-1}) and we could find no transition state for the formation of HSO_2.

The only significant products are therefore SO + OH (R1b) and HSO + O (R1c). The channel forming HSO + O passes through a loose transition state and has a relatively high pre-exponential factor, whereas the formation of SO + OH, which has a lower barrier (by about 8 kJ mol^{-1}), also has a lower pre-exponential factor due to the occurrence of a four-centered transition state. At temperatures below 1000 K, the formation

of SO + OH predominates, but the entropy effects at higher temperatures produce comparable rates for the two channels. As a consequence, the reaction R1b is 2 orders of magnitude faster than R1c at room temperature, revealing that the atmospheric oxidation of SH leads directly to the formation of SO + OH with a rate coefficient of $\sim 1.0 \times 10^{-2}$ cm^3 mol^{-1} s^{-1}.

Acknowledgment. The authors acknowledge the support of the Australian Research Council for part of this work. The computations were performed at Australia Partnership for Advanced Computing (APAC) at the Australian National University, Canberra. Chenlai (Ryan) Zhou thanks the School of Chemical and Biomolecular Engineering of the University of Sydney for the award of the FH Loxton Postgraduate Studentship.

Supporting Information Available: Geometries of all species and transition states presented. This material is available free of charge via the Internet at http://pubs.acs.org.

References and Notes

(1) Black, G. *J. Chem. Phys.* **1984**, *80*, 1103–1107.
(2) Friedl, R. R.; Brune, W. H.; Anderson, J. G. *J. Phys. Chem.* **1985**, *89*, 5505–5510.
(3) Schonle, G.; Rahman, M. M.; Schindler, R. N. *Ber. Bunsen-Ges. Phys. Chem.* **1987**, *91*, 66–75.
(4) Stachnik, R. A.; Molina, M. J. *J. Phys. Chem.* **1987**, *91*, 4603–4606.
(5) Wang, N. S.; Lovejoy, E. R.; Howard, C. J. *J. Phys. Chem.* **1987**, *91*, 5743–5749.
(6) Frenklach, M.; Lee, J. H.; White, J. N.; Gardiner, W. C. *Combust. Flame* **1981**, *41*, 1–16.
(7) Tsuchiya, K.; Kamiya, K.; Matsui, H. *Int. J. Chem. Kinet.* **1997**, *29*, 57–66.
(8) Goumri, A.; Rocha, J. D. R.; Laakso, D.; Smith, C. E.; Marshall, P. *J. Phys. Chem. A* **1999**, *103*, 11328–11335.
(9) Goumri, A.; Rocha, J. D. R.; Marshall, P. *J. Phys. Chem.* **1995**, *99*, 10834–10836.
(10) Resende, S. M.; Ornellas, F. R. *Phys. Chem. Chem. Phys.* **2003**, *5*, 4617–4621.
(11) Ballester, M. Y.; Varandas, A. J. C. *Phys. Chem. Chem. Phys.* **2005**, *7*, 2305–2317.
(12) Ballester, M. Y.; Guerrero, Y. O.; Garrido, J. D. *Int. J. Quantum Chem.* **2008**, *108*, 1705–1713.
(13) Sendt, K.; Haynes, B. S. *Proc. Combust. Inst.* **2007**, *31*, 257–265.
(14) Zhou, C.; Sendt, K.; Haynes, B. S. *J. Phys. Chem. A* **2008**, *112*, 3239–3247.
(15) Langhoff, S. R.; Davidson, E. R. *Int. J. Quantum Chem.* **1974**, *8*, 61–72.
(16) Dunning, T. H.; Peterson, K. A.; Wilson, A. K. *J. Chem. Phys.* **2001**, *114*, 9244–9253.
(17) Bauschlicher, C. W.; Partridge, H. *Chem. Phys. Lett.* **1995**, *240*, 533–540.
(18) Werner, H.-J.; Lindh, P. J. K. R. Manby, F. R.; Schütz, M.; Celani, P.; Korona, T.; Rauhut, G. Amos, R. D. Bernhardsson, A. Berning, A.; Cooper, D. L.; Deegan, M. J. O. Dobbyn, A. J.; Eckert, F. Hampel, C. Hetzer, G. Lloyd, A. W.; McNicholas, S. J.; Meyer, W.; Mura, M. E. Nicklass, A. Palmieri, P.; Pitzer, R.; Schumann, U.; Stoll, H. Stone, A. J. Tarroni, R. Thorsteinsson, T. *MOLPRO*, version 2006.1, A package of ab initio programs, see http://www.molpro.net.
(19) *DALTON*, A molecular electronic structure program, Release 2.0 (2005), see http://www.kjemi.uio.no/software/dalton/dalton.html.
(20) Frisch, M. J. ; Trucks, G. W.; Schlegel, H. B.; Scuseria, G. E.; Robb, M. A.; Cheeseman, J. R.; Zakrzewski, V. G.; Montgomery, J. A., Jr.; Stratmann, R. E.; Burant, J. C.; Dapprich, S.; Millam, J. M.; Daniels, A. D.; Kudin, K. N.; Strain, M. C.; Farkas, O.; Tomasi, J.; Barone, V.; Cossi, M.; Cammi, R.; Mennucci, B.; Pomelli, C.; Adamo, C.; Clifford, S.; Ochterski, J.; Petersson, G. A.; Ayala, P. Y.; Cui, Q.; Morokuma, K.; Malick, D. K.; Rabuck, A. D.; Raghavachari, K.; Foresman, J. B.; Cioslowski, J.; Ortiz, J. V.; Stefanov, B. B.; Liu, G.; Liashenko, A.; Piskorz, P.; Komaromi, I.; Gomperts, R.; Martin, R. L.; Fox, D. J.; Keith, T.; Al-Laham, M. A.; Peng, C. Y.; Nanayakkara, A.; Gonzalez, C.; Challacombe, M.; Gill, P. M. W.; Johnson, B. G.; Chen, W.; Wong, M. W.; Andres, J. L.; Head-Gordon, M.; Replogle, E. S.; Pople, J. A. *Gaussian 98*, Revision A.9 ed; Gaussian, Inc., Pittsburgh PA: 1998.
(21) Wigner, E. *Z. Phys. Chem. B* **1932**, *19*, 203–216.
(22) Laakso, D.; Smith, C. E.; Goumri, A.; Rocha, J. D. R.; Marshall, P. *Chem. Phys. Lett.* **1994**, *227*, 377–383.
(23) Gorin, E. *Acta Physiochim URSS* **1938**, *9*, 691.
(24) Gurvich, L. V.; Veyts, I. V.; Alcock, C. B. *Thermodynamic Properties of Individual Substances*, Fourth Edition; Hemisphere: New York, 1989.
(25) Chase, M. W. Thermochemical Tables Fourth Edition. *J. Phys. Chem. Ref. Data* **1998**, Monograph No. 9.
(26) Shiell, R. C.; Hu, X. K.; Hu, Q. J.; Hepburn, J. W. *J. Phys. Chem. A* **2000**, *104*, 4339–4342.
(27) Denis, P. A. *Chem. Phys. Lett.* **2005**, *402*, 289–293.
(28) Ruscic, B.; Pinzon, R. E.; Morton, M. L.; Srinivasan, N. K.; Su, M. C.; Sutherland, J. W.; Michael, J. V. *J. Phys. Chem. A* **2006**, *110*, 6592–6601.

JP810105E